

## Supporting Information

### **Structural and photo physical investigation of single-source evaporation of CsFAPbI<sub>3</sub> and FAPbI<sub>3</sub> perovskite thin films**

Nadja Klipfel<sup>1</sup>, Muhammed P U Haris<sup>2</sup>, Samrana Kazim<sup>2,5</sup>, Albertus Adrian Sutanto<sup>1</sup>,  
Naoyuki Shibayama<sup>3</sup>, Hiroyuki Kanda<sup>1</sup>, Abdullah M. Asiri,<sup>4</sup> Cristina Momblona<sup>1\*</sup>, Shahzada  
Ahmad<sup>2,5\*</sup>, Mohammad Khaja Nazeeruddin<sup>1,6\*</sup>

<sup>1</sup>*Group for Molecular Engineering of Functional Materials, Institute of Chemical Sciences and Engineering, École Polytechnique Fédérale de Lausanne, Valais Wallis, Rue de l'Industrie 17, 1950 Sion, Switzerland.*

<sup>2</sup>*BCMaterials, Basque Center for Materials, Applications, and Nanostructures, UPV/EHU Science Park, Leioa, 48940 Spain.*

<sup>3</sup>*Department of Biomedical Engineering, Tooin University of Yokohama, 1614 Kurogane, Aoba, Yokohama, Japan.*

<sup>4</sup>*Center of Excellence for Advanced Materials Research (CEAMR), King Abdulaziz University, P.O. Box 80203, 21589 Jeddah, Saudi Arabia.*

<sup>5</sup>*IKERBASQUE, Basque Foundation for Science, Bilbao 48009, Spain.*

<sup>6</sup>*Department of Materials Science and Engineering, City University of Hong Kong, Kowloon, Hong Kong.*

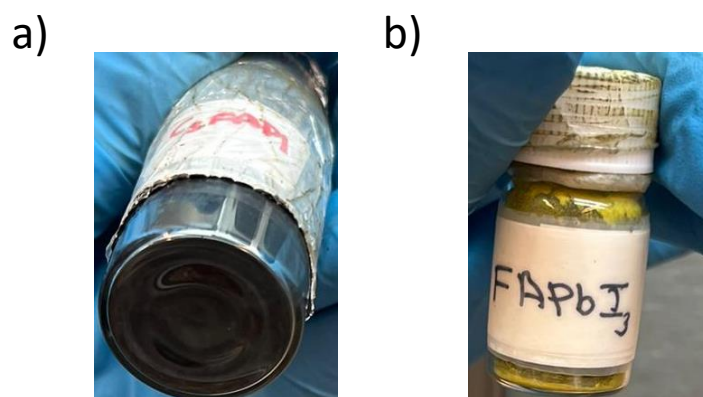


Figure S1: Photographs of the pre-synthesized perovskite material used for the single-source evaporation a)  $\alpha$ -CsFAPbI<sub>3</sub> powder and b)  $\delta$ -FAPbI<sub>3</sub> powder

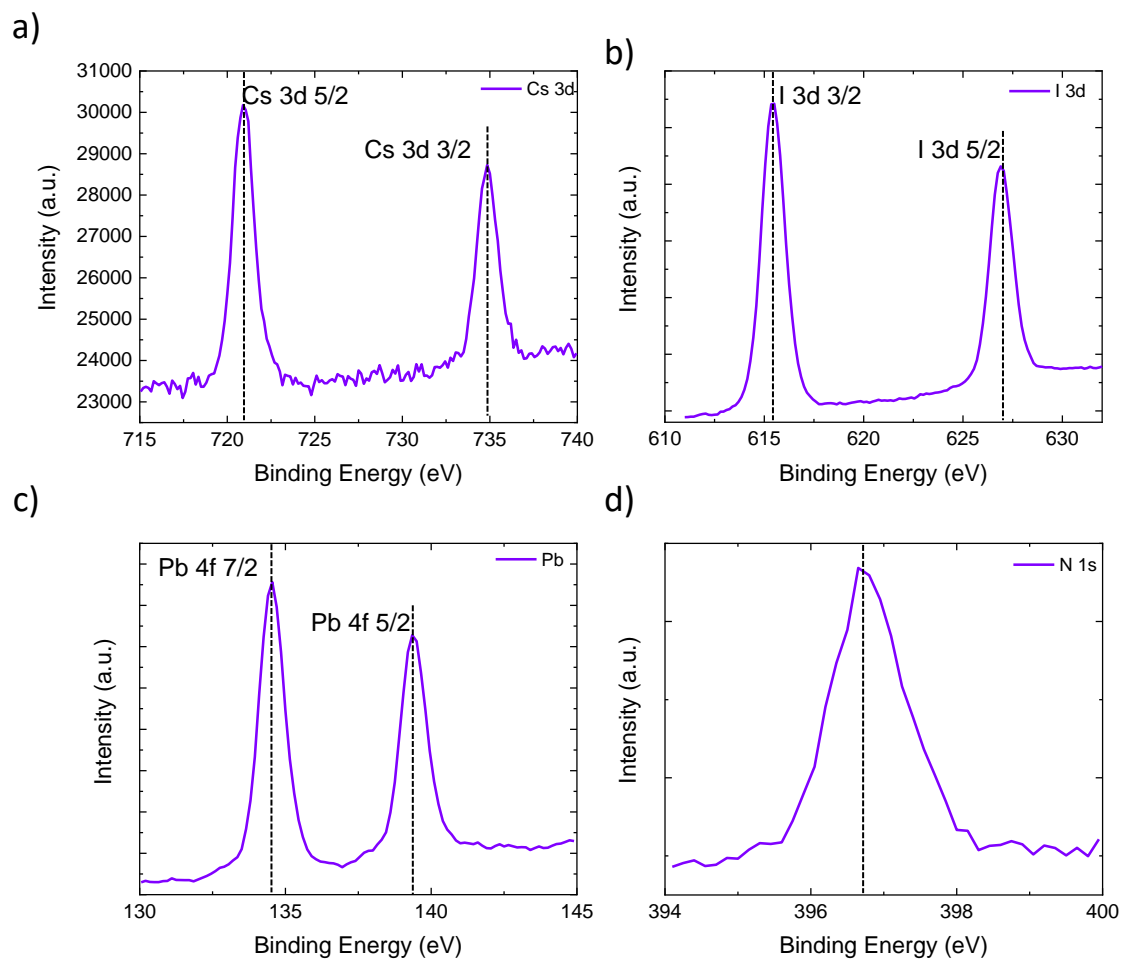


Figure S2. XPS spectra of pre-synthesized  $\alpha$ -CsFAPbI<sub>3</sub> powder. a) Cs 3d; b) I 3d; c) Pb 4f; d) N 1s.

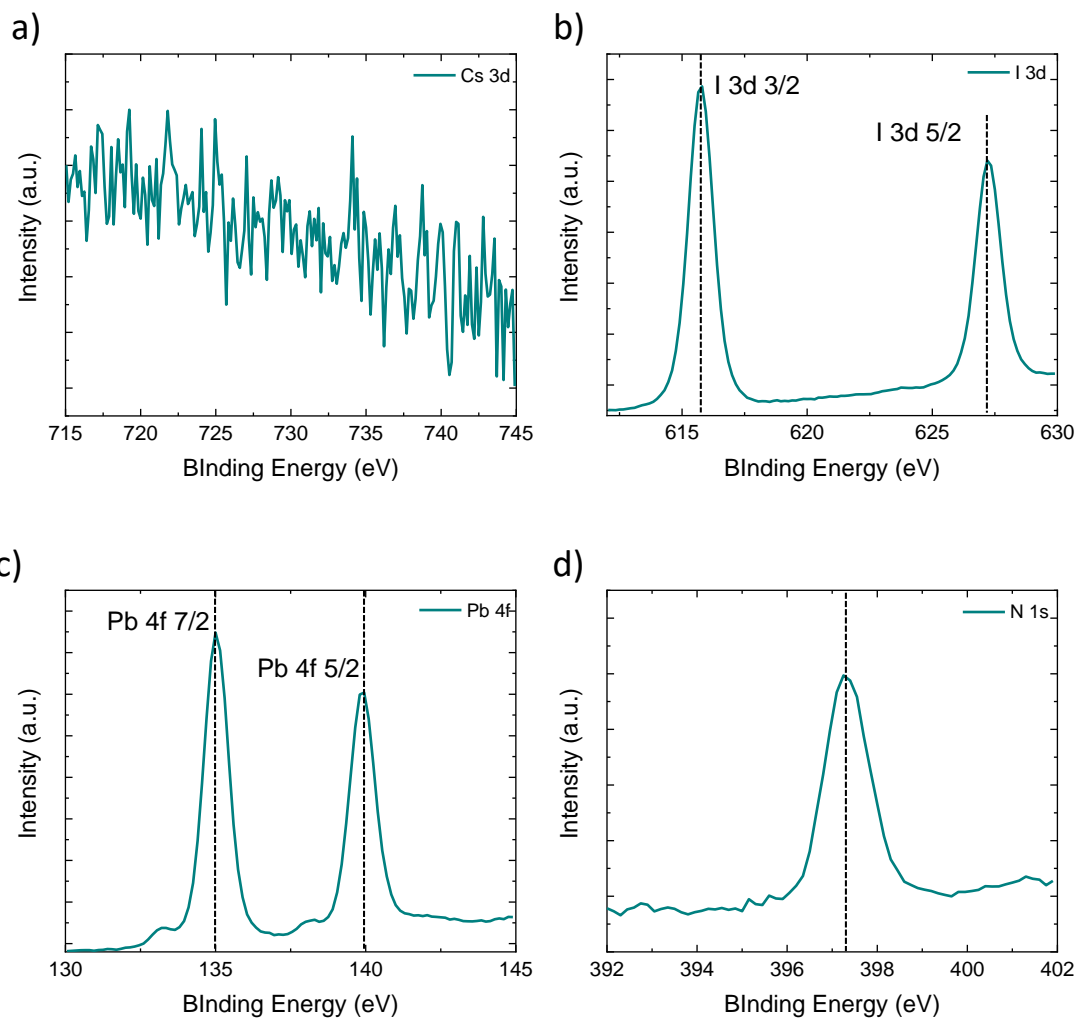


Figure S3. XPS spectra of pre-synthesized  $\delta$ -FAPbI<sub>3</sub> powder. a) Cs 3d b) I 3d c) Pb 4f d) N 1s.

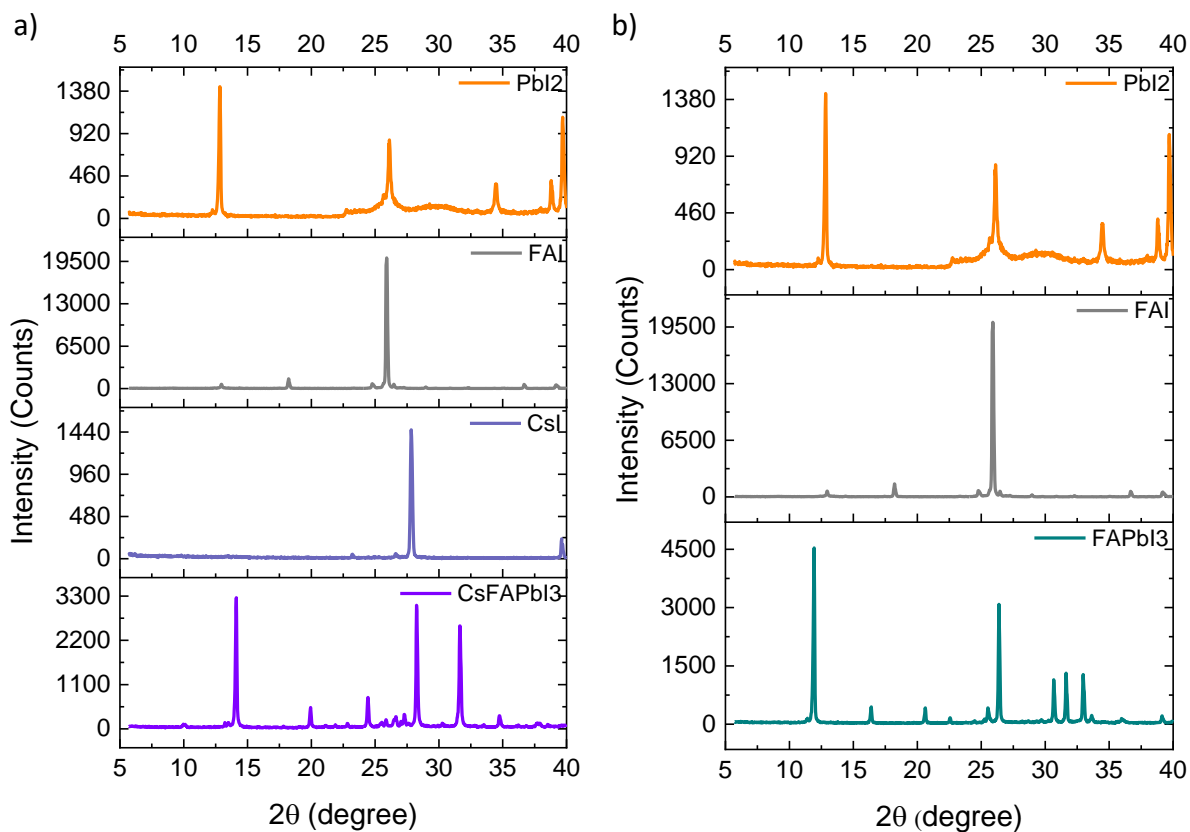


Figure S4. The phase purity of synthesized powders and their precursor materials a)  $\alpha$ -CsFAPbI<sub>3</sub> powder, and b)  $\delta$ -FAPbI<sub>3</sub> powder.

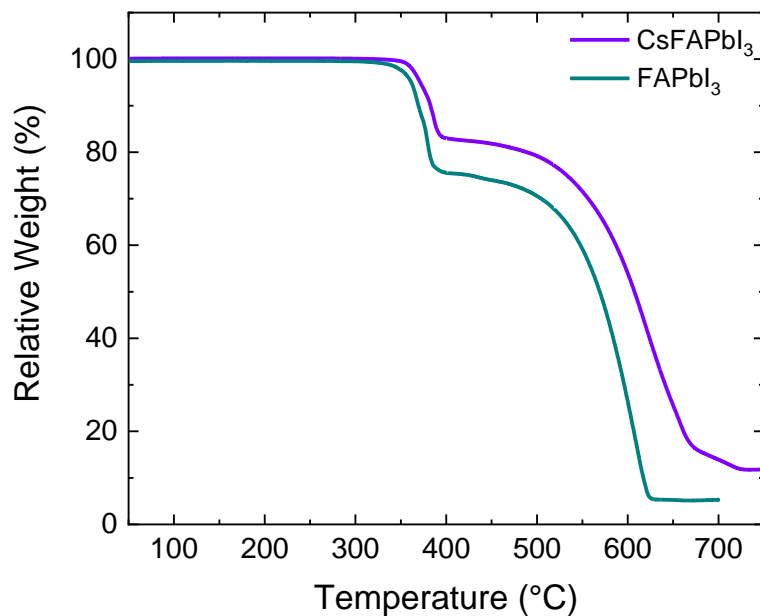

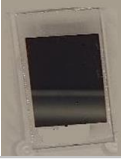





Figure S5: TGA of pre-synthesized CsFAPbI<sub>3</sub> and FAPbI<sub>3</sub> powders.

Table S1: Vacuum deposited rate correlated to crystal phase perovskite from pre-synthesized powder and the corresponding image of the deposited film.

perovskite powder	deposition rate, Å/s	phase	photograph of the as-deposited layer
<b>CsFAPbI<sub>3</sub></b>	0.25	$\delta/\alpha$	
	0.35	$\alpha$	
	1.0-1.05	$\delta$	
<b>FAPbI<sub>3</sub></b>	1.0-1.05	$\delta$	
	3.0-3.05	$\alpha/\delta$	

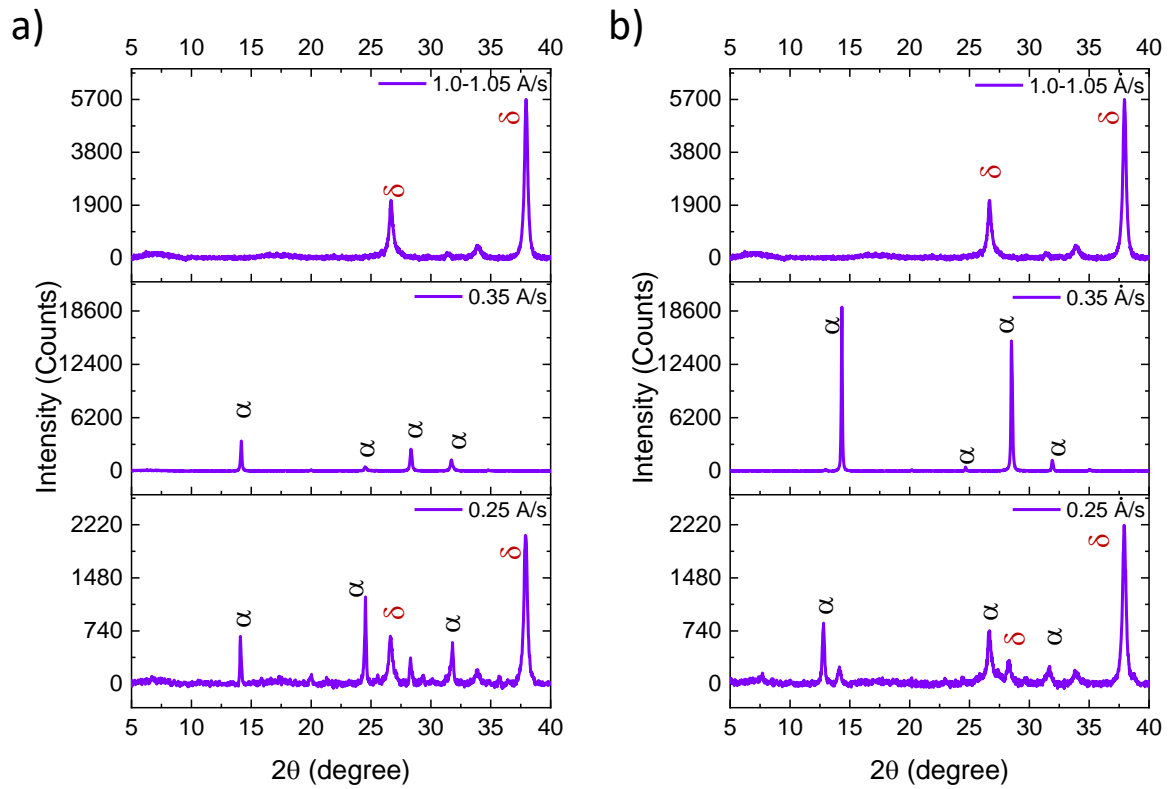


Figure S6: a) XRD pattern of deposited thin film at a rate of 1.0-1.05 Å/s, 0.35 Å/s, 0.25 Å/s. a) as deposited, and b) after annealing. Planes in black indicate α-CsFAPbI<sub>3</sub>, planes in brown represents δ-CsFAPbI<sub>3</sub>.

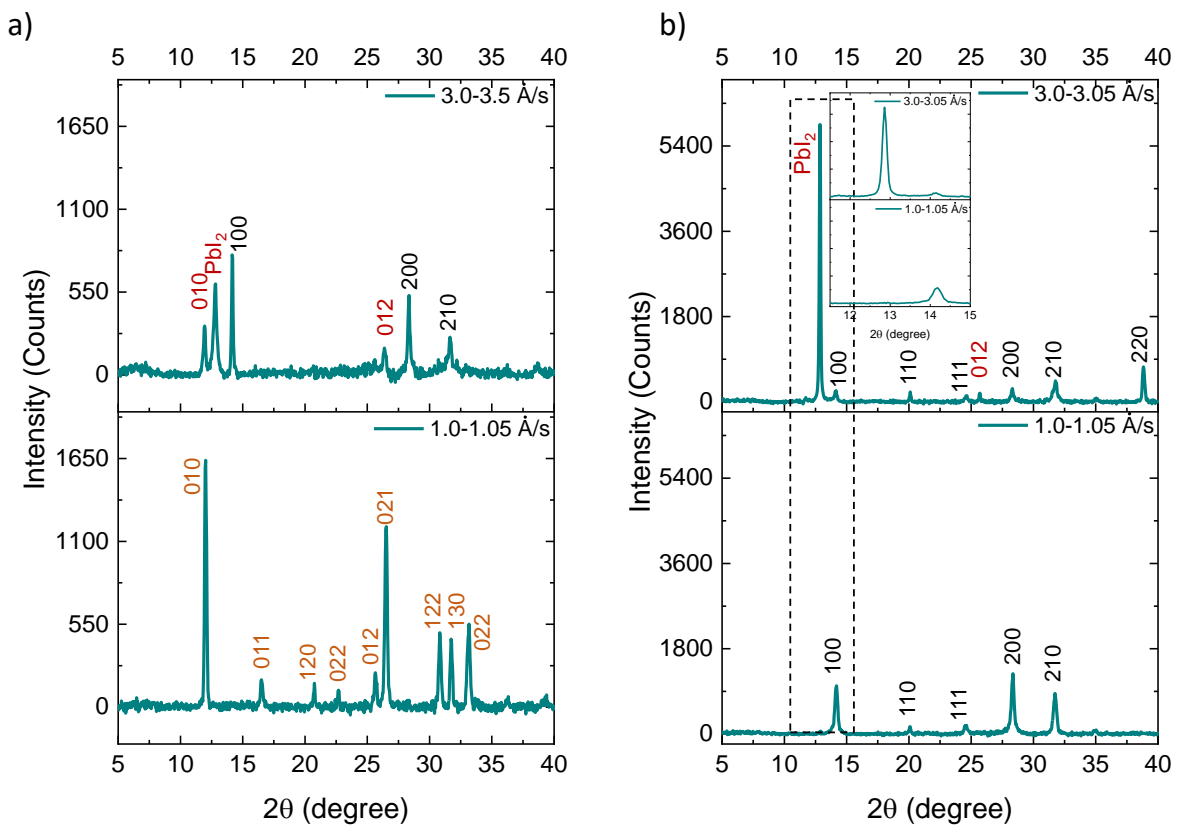


Figure S7: XRD pattern of deposited thin film at a rate of 1.0-1.05 Å/s 3.0-3.05 Å/s, a) as deposited, and b) after annealing. Planes in black indicate  $\alpha$ -FAPbI<sub>3</sub>, planes in brown represents  $\delta$ -FAPbI<sub>3</sub>.

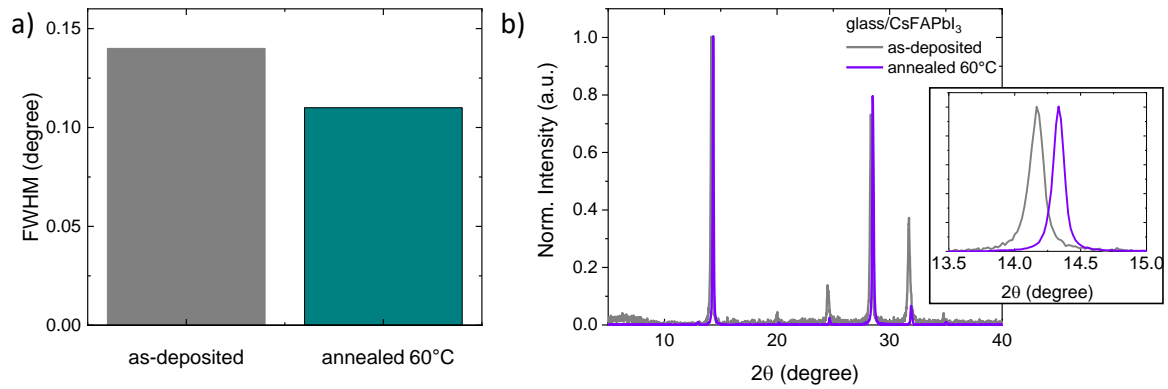


Figure S8: a) FWHM values for perovskite  $\alpha$ -phase thin films, b) XRD pattern suggesting shift for  $\alpha$ -phase thin films.

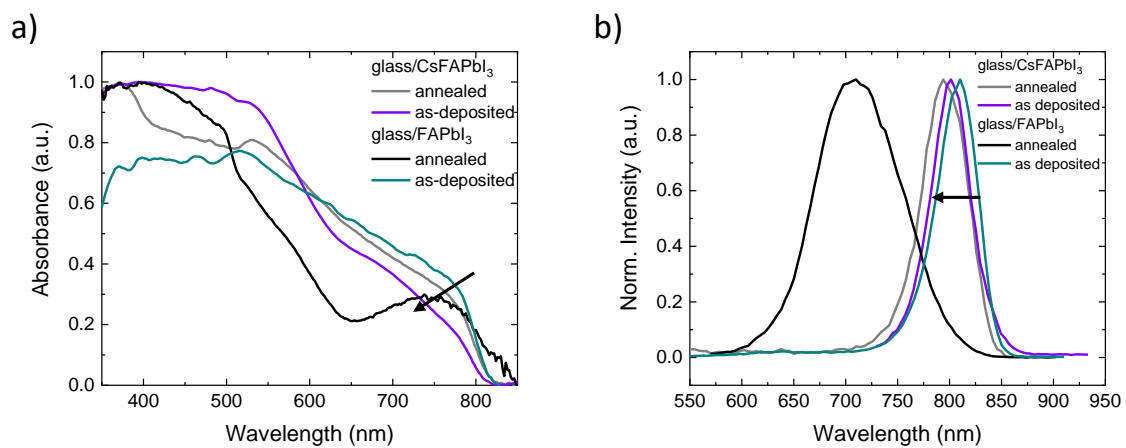


Figure S9. a) UV/Vis spectra of CsFAPbI<sub>3</sub> (deposited at 0.35 Å/s), and FAPbI<sub>3</sub> (deposited at 1.01.05 Å/s), on glass substrate as-deposited and after annealing, b) PL spectra of the corresponding CsFAPbI<sub>3</sub>, and FAPbI<sub>3</sub> perovskite films, on glass substrate as-deposited and after annealing.

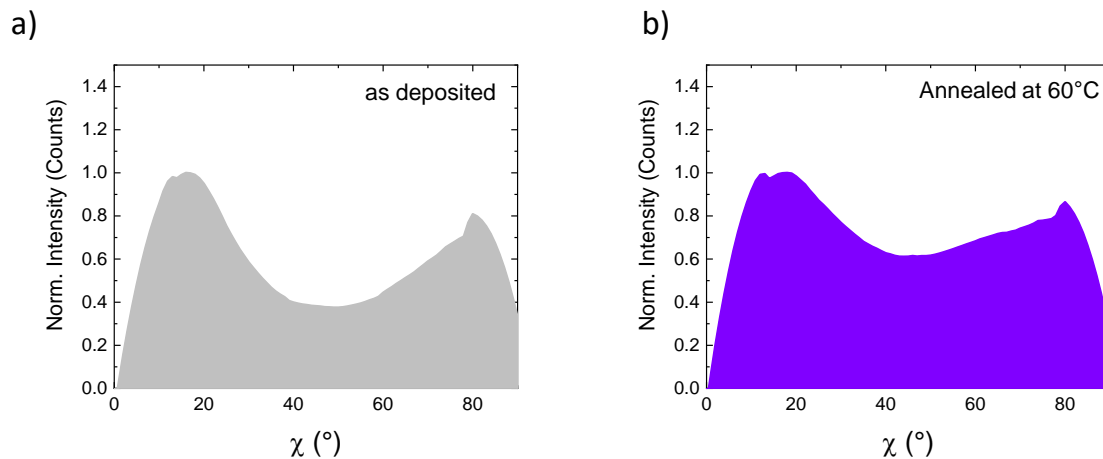


Figure S10: Integration of the azimuthal intensity along 100 reflex ( $1.0\text{\AA}^{-1}$ ) of GIWAXS images shown in Figures 2 a, b a) of the as-deposited CsFAPbI<sub>3</sub> film, and b) of the CsFAPbI<sub>3</sub> film annealed at 60°C.

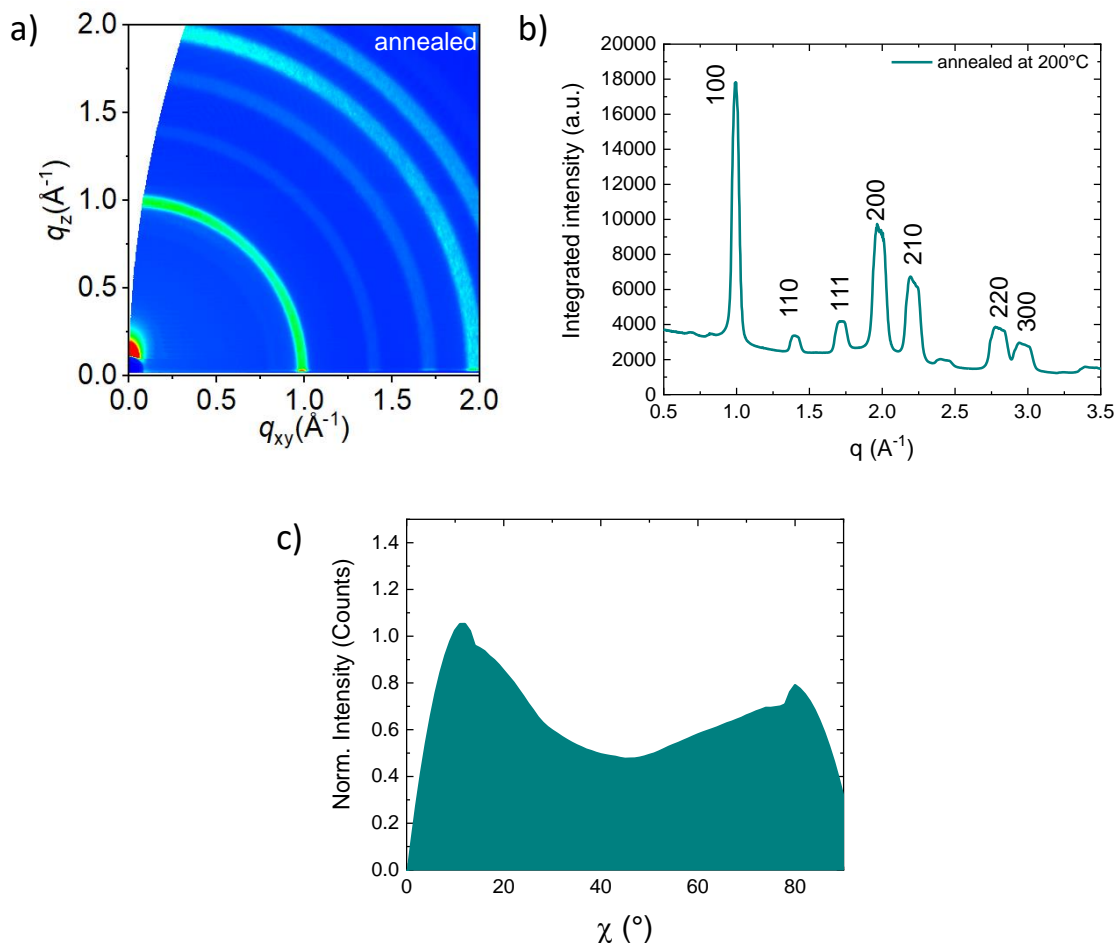


Figure S11: GIWAXS images taken at an angle of 0.12 for a) as deposited FAPbI<sub>3</sub> film and annealed at 200°C, b) Integrated  $q$ -data of the GIWAXS images for FAPbI<sub>3</sub> film after post-annealing at 200°C, and c) Integration of the azimuthal intensity along 100 reflex ( $1.0\text{\AA}^{-1}$ ) of GIWAXS images of annealed FAPbI<sub>3</sub> film.



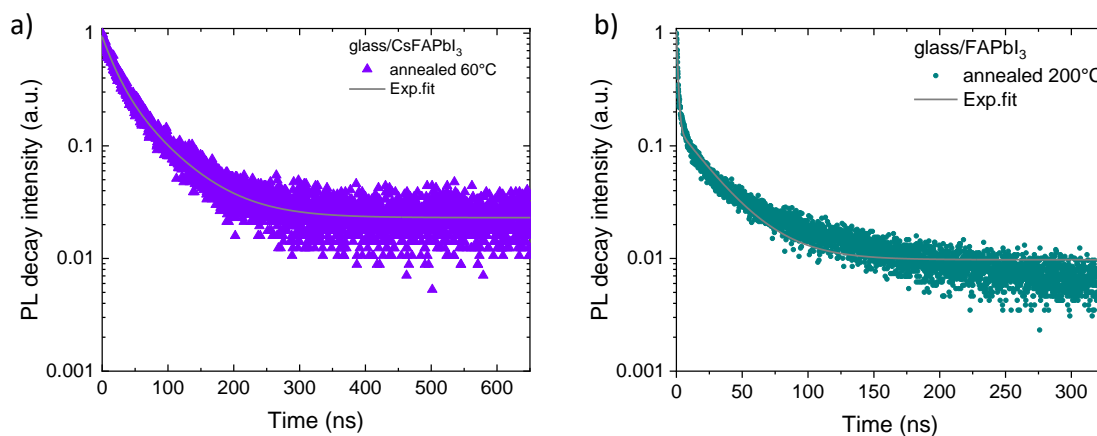


Figure S12: Time resolved photoluminescence spectra (TRPL) for annealed, a)  $\alpha$ -CsFAPbI<sub>3</sub> films, and b) FAPbI<sub>3</sub>.

Table S2: Fitted decay parameters extracted from time-resolved photoluminescence (TRPL) spectra for annealed thin films.

Name	$\tau_1$ (ns)	$\tau_2$ (ns)
$\alpha$ -CsFAPbI <sub>3</sub>	18.89±0.45	61.61±1.24
$\alpha$ -FAPbI <sub>3</sub>	1.09±0.01	27.03±0.25

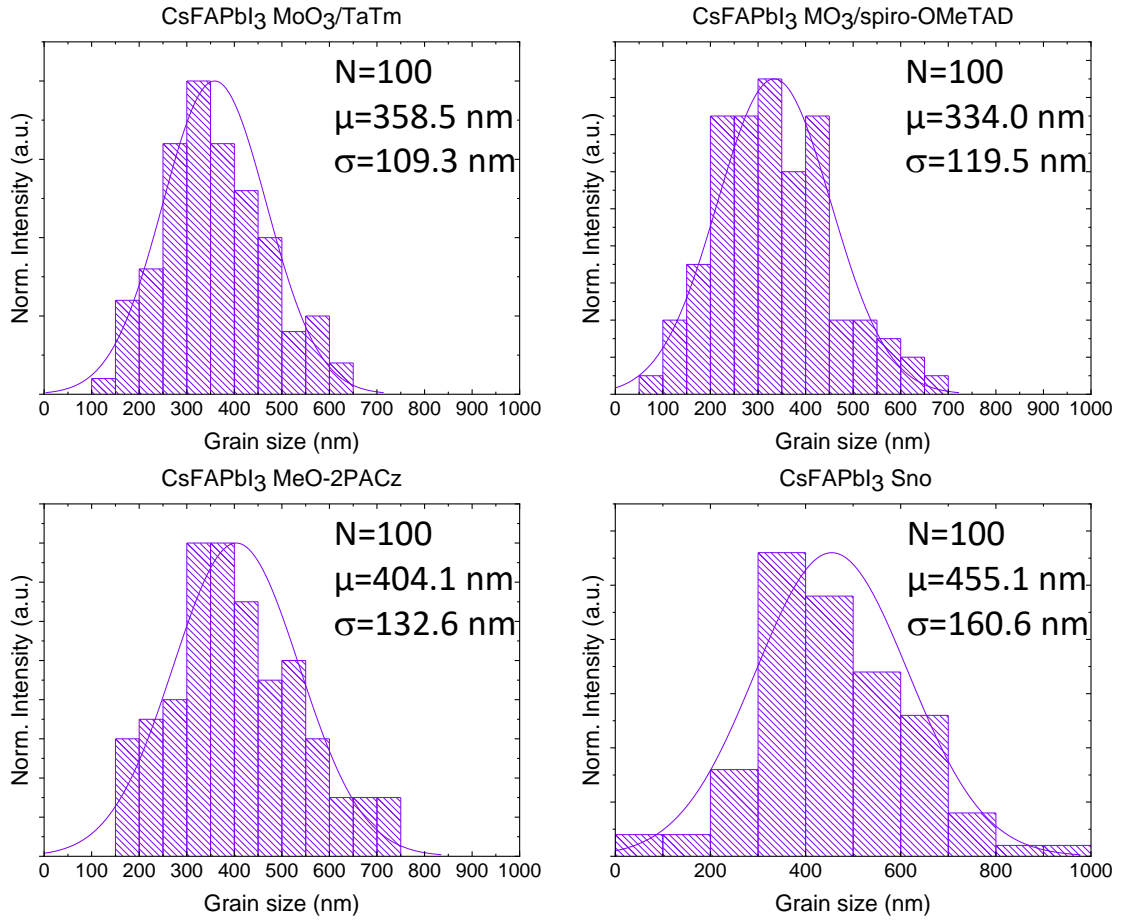


Figure S13: Grain size distribution extracted from top-view SEM images for  $\alpha$ -CsFAPbI<sub>3</sub> on top of the different under layers.

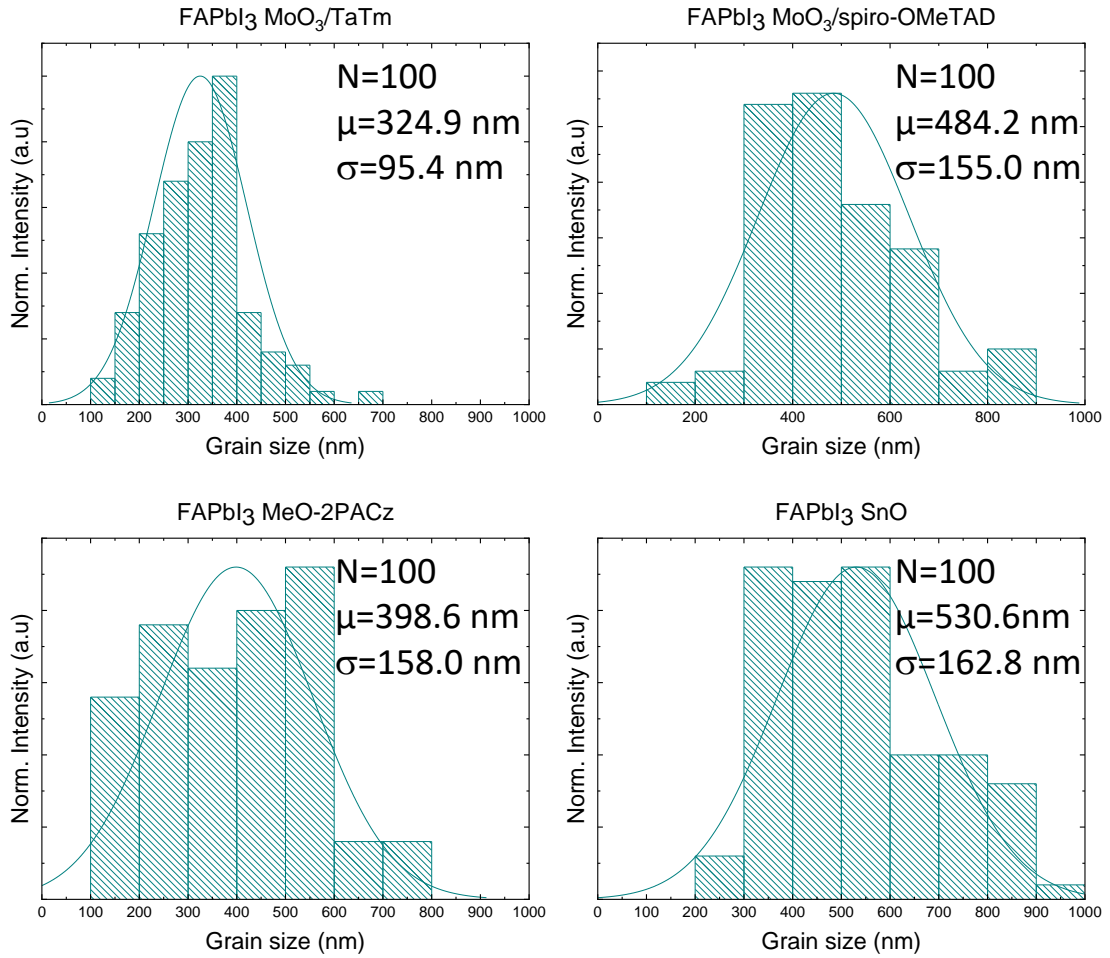


Figure S14: Grain size distribution extracted from top-view SEM images for  $\alpha$ -FAPbI<sub>3</sub> on top of the different under layers.

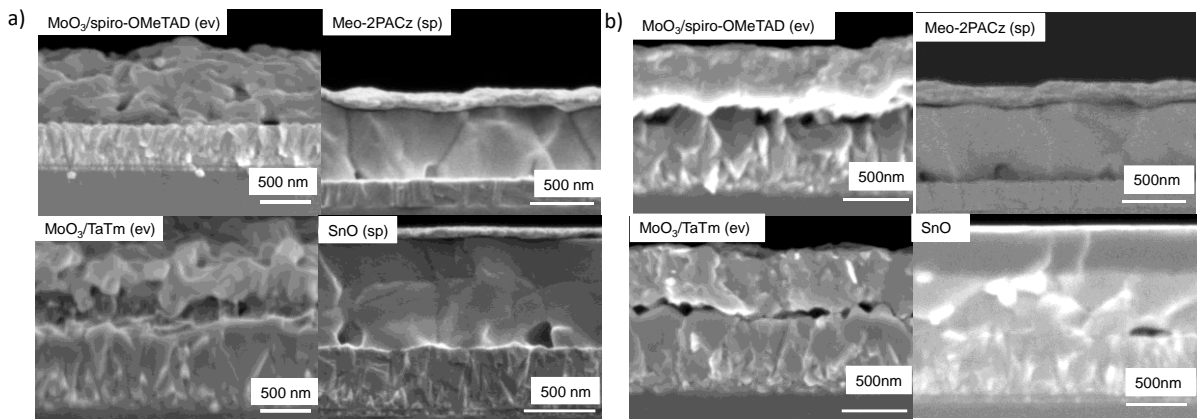


Figure S15: Cross-section SEM images of annealed perovskite deposited on different underlayers, (a) cross-section SEM of  $\alpha$ -CsFAPbI<sub>3</sub> ( $0.35 \text{ \AA s}^{-1}$ ) (b) cross-section SEM of  $\alpha$ -FAPbI<sub>3</sub>, ( $1.0\text{--}1.05 \text{ \AA s}^{-1}$ ): (ev) = evaporated layer and (sp) = spin-coated layer deposited at  $0.35 \text{ \AA s}^{-1}$ .

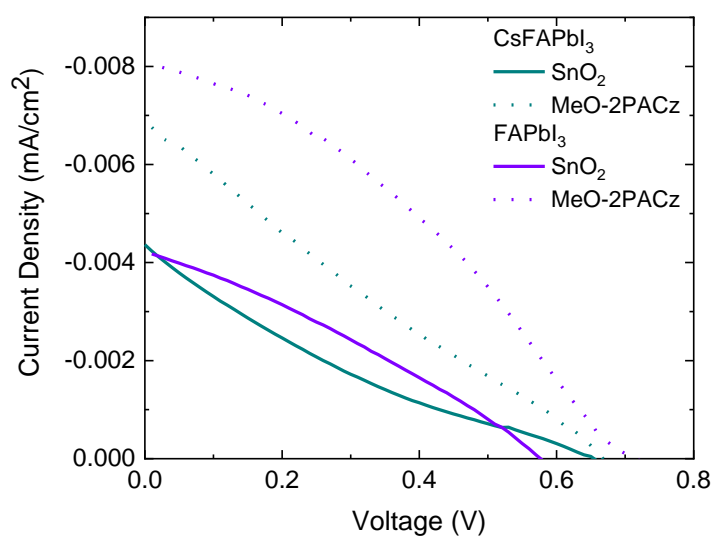


Figure S16: J-V curves for the best efficient devices fabricated with CsFAPbI<sub>3</sub> or FAPbI<sub>3</sub> using SnO<sub>2</sub> or MeO-2PACz as charge transporting layers.

Table S3: PV parameters extracted from the JV curves of the most efficient PSCs.

Structure	V <sub>oc</sub> (V)	J <sub>sc</sub> (mA/cm <sup>2</sup> )	FF	PCE (%)
FTO/SnO <sub>2</sub> /FAPbI <sub>3</sub> /doped spiro-OMeTAD/Au	0.693	2.91	0.32	0.63
FTO/MeO-2PACz/FAPbI <sub>3</sub> /C <sub>60</sub> /BCP/Cr/Au	0.715	8.08	0.34	1.94
FTO/SnO <sub>2</sub> /CsFAPbI <sub>3</sub> /Spiro-OMeTAD/Au	0.655	4.58	0.24	0.74
FTO/MeO-2PACz/CsFAPbI <sub>3</sub> /C <sub>60</sub> /BCP/Cr/Au	0.668	6.89	0.23	1.06